Toward Single-DNA Electrochemical Biosensing by Graphene Nanowalls

Omid Akhavan,[†,‡,*] Elham Ghaderi,[†] and Reza Rahighi[†]

[†]Department of Physics, Sharif University of Technology, P.O. Box 11155-9161, Tehran, Iran and [‡]Institute for Nanoscience and Nanotechnology, Sharif University of Technology, P.O. Box 14588-89694, Tehran, Iran

ABSTRACT

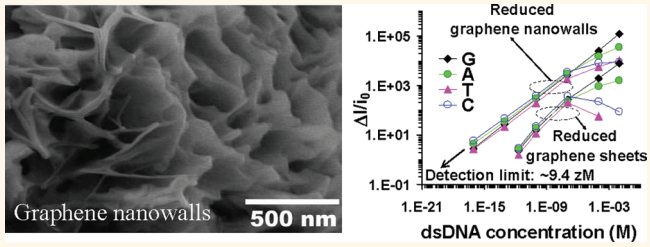

Graphene oxide nanowalls with extremely sharp edges and preferred vertical orientation were deposited on a graphite electrode by using electrophoretic deposition in an Mg^{2+}-GO electrolyte. Using differential pulse voltammetry (DPV), reduced graphene nanowalls (RGNWs) were applied for the first time, in developing an ultra-high-resolution electrochemical biosensor for detection of the four bases of DNA (G, A, T, and C) by monitoring the oxidation signals of the individual nucleotide bases. The extremely enhanced electrochemical reactivity of the four free bases of DNA, single-stranded DNA, and double-stranded DNA (dsDNA) at the surface of the RGNW electrode was compared to electrochemical performances of reduced graphene nanosheet (RGNS), graphite, and glassy carbon electrodes. By increasing the number of DPVs up to 100 scans, the RGNW electrode exhibited an excellent stability with only 15% variation in the oxidation signals, while for the RGNS electrode no detectable signals relating to T and C of 0.1 μM dsDNA were observed. The linear dynamic detection range of the RGNW electrode for dsDNA was checked in the wide range of 0.1 fM to 10 mM, while for the RGNS electrode, it was from 2.0 pM to <10 mM. The lower limits of dsDNA detection of the RGNW and RGNS electrodes were estimated as 9.4 zM (~5 dsDNA/mL) and 5.4 fM, respectively. The RGNWs were efficient in label-free detection of single nucleotide polymorphisms of 20 zM oligonucleotides (~10 DNA/mL) having a specific sequence. Therefore, the RGNWs can effectively contribute to the development of ultra-high-sensitive electrochemical biosensors with single-DNA resolutions.

KEYWORDS: graphene · nanowalls · biosensors · electrochemistry · DNA · nucleotide bases · detection limit

Carbon-based nanostructures such as carbon nanofibers,[1] carbon nanotubes (CNTs),[2] and mesoporous carbons[3] have been extensively used in fabrication of modified electrodes for applications in both analytical and industrial electrochemistry, because in addition to their low price, they exhibit suitable electrocatalytic activity for a variety of redox reactions, a broad potential window, and relatively inert electrochemistry.[4,5] Recently, the most fascinating nanomaterial in physics with unique and promising properties in both scientific[6−11] and technological[12−19] aspects is graphene, as the first realization of a single-atom-thick sheet.[20]

There is also increasing interest in the application of graphene-based materials in bioelectronics, biosensing, and biology. For instance, graphene-based materials were utilized in biosensors,[21−25] glucose sensors,[26−29] single-bacterium sensors and DNA transistors,[30] and sensitive immunosensors for cancer biomarkers[31] and for antimicrobial purposes.[32−36]

In the field of biosensors, sequence-specific detection of very small amounts of DNA has been attracting much attention in a broad range of applications such as food safety testing, clinical diagnostics, and forensics. In these applications, the concentration of nucleic acids that are attainable from samples falls typically below 20 fM.[37,38] In this regard, electrochemical sensing of DNA with many approaches is one of the most attractive and promising techniques, because it can provide sensitive, fast, facile, and low-cost detection of small volumes of DNA in miniaturized devices. For example, it was shown that label-free electrochemical detection of DNA based on a gold nanoparticles/poly(neutral red)-modified electrode can yield the lower detection limit of 4.2 pM.[39] In another work with a better sensitivity, Zhang *et al.*[40] reported a femtomolar resolution chronocoulometric DNA sensor based on a "sandwich" detection scheme, which includes capture probe DNA immobilized on gold electrodes and reporter probe DNA labeled with gold nanoparticles that flank the target DNA sequence. Ren *et al.*[41] also constructed a chronocoulometric DNA sensor based on a screen-printed electrode doped with ionic

* Address correspondence to oakhavan@sharif.edu.

Received for review August 8, 2011 and accepted March 3, 2012.

Published online March 04, 2012
10.1021/nn300261t

liquid and polyaniline nanotubes with a detection limit of ~0.08 fM. As a record thus far, Ferguson *et al.*[42] showed that their integrated microfluidic electrochemical DNA sensor could detect genomic DNA of *Salmonella enterica* serovar Typhimurium LT2 with a detection limit of <10 aM (1 atto = 10^{-18}), which is ~2 orders of magnitude lower than that of previously reported electrochemical chip-based methods.[42]

In addition to the electrochemical sensing methods, there are also other approaches for DNA detection. For example, electronic DNA detection schemes provided detection limits ranging from ~1 pM to 0.1 fM.[43,44] In this regard, very recently, Bangar *et al.*[45] reported a label-free single polypyrrole nanowire-based conductometric/chemiresistive DNA sensor with a lower detection limit of ~0.1 fM and wide dynamic range of ~0.1 fM to 10 pM. Regarding optical DNA sensors, Peter *et al.*[46] developed an optical sensor system based on evanescent field excitation of fluorophore-labeled DNA targets specifically binding to immobilized DNA probes with a lower detection limit of 0.2 nM. Recently, Gnanaprakasa *et al.*[47] developed an optical DNA biosensor with a detection limit of 2.5 nM using direct covalent coupling of thiol- and biotin-labeled DNA on the surface plasmon resonance of a transduction platform. As one of the best results ever attained, Loaiza *et al.*[48] developed a magnetic DNA sensor using an enzyme-amplified strategy for attomolar detection of a gene related to the *Enterobacteriaceae* bacterial family, based on coupling of streptavidin-peroxidase to biotinylated *lacZ* gene target sequences.

Among the various methods for DNA electrochemical analysis,[49,50] direct oxidation of DNA is known as one of the simplest ones,[51−55] which can also provide rapid and sensitive detection of single nucleotide polymorphisms (SNPs).[55,56] However, due to some of its drawbacks originating from the relatively narrow potential window, high background current, and/or slow electron exchange of many electrode materials,[53−55] up to now, only electron cyclotron resonance of nanocarbon films[55] and graphene-based materials[56−58] could realize a simultaneous detection of all four DNA bases, *i.e.*, guanine (G), adenine (A), thymine (T), and cytosine (C). The successful application of graphene in electrochemical sensing of DNA is attributed to its highly efficient two-dimensional (2D) electrical conduction originating from the in-plane sp^2-hybridized structure of the sheets. Due to such 2D structure, heterogeneous electron exchange with redox species in an electrochemical process can occur substantially through the sharp edges of the graphene sheets, while it should be negligible through the basal plane of the graphene sheet.

The first study concerning simultaneous electrochemical sensing of all four DNA bases by graphene-based electrodes was reported by Zhou *et al.*[56] They demonstrated that a chemically reduced graphene oxide modified glassy carbon electrode can electrochemically detect the four DNA bases in both single-stranded DNA (ssDNA) and double-stranded DNA (dsDNA) with a concentration of ~1 μM at the physiological pH of 7.0 without a prehydrolysis step.[56] After that, Lim *et al.*[57] showed that graphene nanosheets epitaxially grown on SiC could present a better electrochemical response to the DNA bases of dsDNA (with a concentration 3 times greater than the concentration used by Lim *et al.*[56]) by increasing the edge-plane-like defective sites of the nanosheets through anodizing of the epitaxial graphene film. Very recently, Dubuisson *et al.*[58] showed that based on direct oxidation of nucleotide bases, the anodized epitaxial graphene electrode can also detect the four DNA bases of ssDNA at a low concentration of 1 nM (the lowest DNA concentration used so far in the direct oxidation sensing). In addition, using electrochemical impedance spectroscopy they indicated that the anodized epitaxial graphene electrode can exhibit a wide linear dynamic detection range from 50 fM to 1 μM for DNA oligonucleotides (not its nucleic acids).[58] However, the dynamic detection range of the four bases of DNA through direct electrooxidation of nucleotide bases has not been studied yet. In addition, although in these works it was shown that the high density of edge-plane-like defective sites on graphene nanosheets provided active sites for accelerating heterogeneous electron transfer between the electrode and DNA species,[56,57] so far no investigation on electrooxidation of the four DNA bases by using vertical (not parallel) graphene nanoflakes (which can provide a porous structure with extraordinary edge plane defects for a more efficient heterogeneous electron exchange and better electrochemical sensitivity) has been reported. There is only one report on fast, sensitive, and simultaneous electrochemical sensing of dopamine, ascorbic acid, and uric acid by using vertical multilayer graphene nanoflakes grown by a microwave-assisted plasma chemical vapor deposition.[24] The lower limit of the linear dynamic detection of such vertical nanoflakes to dopamine was estimated to be 0.17 μM.[24]

In this work, first, vertical graphene oxide (GO) nanoflakes (here called graphene oxide nanowalls (GONWs)) were deposited on a graphite electrode by using electrophoretic deposition (EPD) in a suspension containing Mg^{2+}-GO nanosheets synthesized by a chemical exfoliation method. The synthesized GONWs were also reduced by hydrazine to obtain reduced graphene nanowalls (RGNWs). Then, the fabricated RGNW electrode with a large surface area and edge-plane defects was applied, for the first time, in developing an ultra-high-resolution electrochemical biosensor for detection of the four bases of DNA (potentially at the level of single DNA) through conventional differential pulse voltammetry (DPV). The extremely enhanced electrochemical reactivity of the four free

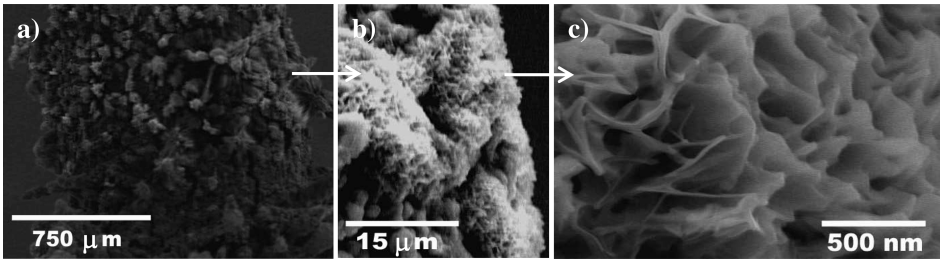

Figure 1. Various magnifications of SEM images of the GONWs deposited on a graphite rod by EPD.

bases of DNA, single-stranded DNA, and double-stranded DNA at the surface of the RGNW electrode was examined and compared to the electrochemical performance of reduced graphene nanosheet, graphite, and glassy carbon (GC) electrodes (as benchmark electrodes). The stability of the oxidation signals of DPVs of the RGNW and RGNS electrodes for detection of 0.1 μM dsDNA was checked and compared. Label-free detection of SNPs of 0.1 nM oligonucleotides having a particular sequence was also investigated by the RGNW electrode. Furthermore, for the first time, the linear dynamic detection range of the RGNW and RGNS electrodes in direct electrooxidation of the individual nucleotide bases of dsDNA in a wide range of concentrations (ranging from 0.1 fM to 10 mM) was investigated to provide potential applications of the RGNWs in developing single-DNA analyses.

RESULTS AND DISCUSSION

Figure 1 shows scanning electron microscope (SEM) images of the GONWs obtained by the EPD on the graphite electrode. Figure 1a shows the graphite electrode after deposition of the GONWs by the EPD. It is seen that the surface of the graphite electrode was uniformly deposited. Using a close-up image (shown in Figure 1b), it was found that most of the surface of the electrode was covered by GONWs. A more magnified close-up image better exhibited the morphology of the GONWs, as presented in Figure 1c. It shows deposition of petal-like graphene nanoflakes with lateral sizes of ~500 nm, extremely sharp edges (with 1−15 nm thickness at the edges), and random directions but with a preferred vertical orientation with respect to the substrate, which all resulted in the formation of a nest-like porous structure with a large surface area. Such vertical nanoflakes may present unique electrochemical properties due to the formation of a large fraction of graphitic edge-plane defects, which can provide a higher surface activity than the graphene nanoflakes deposited parallel to the substrate, *i.e.*, the GONSs in this work (an atomic force microscopic (AFM) image of the GONSs is presented in Figure S1). Therefore, the RGNW electrodes can be applied as promising nanostructures in designing, for example, highly sensitive electrochemistry-based biosensors. It should be noted that reduction of the nanoflakes by hydrazine resulted in no considerable changes in the morphology of the nanoflakes, as also previously reported for graphene nanowalls with the same morphology.[33] Recently, a similar morphology for copper oxide nanoflakes[59] and nanostructured Pd microelectrodes[60] was applied for highly sensitive detection of bacteria and nucleic acids, respectively.

Figure 2a shows DPVs of the RGNW, GONW, RGNS, and GONS electrodes as compared to the DPVs of the graphite and GC electrodes for detection of the four free bases of DNA (G, A, T, and C) with a concentration of 0.1 μM for each one of the species in 0.1 M phosphate-buffered saline (PBS) as supporting electrolyte. It is seen that the height of the current peaks of the various electrodes increased as follows: RGNW > GONW > RGNS > GONS > GC > graphite. In addition, the oxidizing potential of each of the DNA bases on the surface of the various electrodes showed a decrease as follows: RGNW < GONW < RGNS < GONS < GC < graphite. Higher current and lower anodic potential of the graphene-based electrodes indicated their higher electrochemical activity for oxidation of G, A, T, and C, as compared to the corresponding characteristics of the GC and graphite electrodes. The higher electrochemical activity of the graphene-based electrodes can be assigned to better electron exchange between the four free bases and the edge-plane-like defective sites of the reduced graphene sheets as active sites for oxidation of the DNA bases. In fact, substantial removal of the oxygen-containing functional groups from the surface of the GONSs and GONWs after reduction by hydrazine was confirmed by using X-ray photoelectron spectroscopy (XPS), as presented in Figure S2. Our Raman analysis (see Figure S3) also indicated that the graphene nanowalls (GONWs and RGNWs) can provide higher defects than graphene sheets (GONSs and RGNSs). Moreover, reduction by hydrazine increased further defects in the RGNWs as compared to the GONWs (compare Figure S3c,d). These results indicated that the electrochemical performance of the graphene-based electrodes depends on deoxygenation of the electrodes, resulting in a better electron transfer and structural defects providing suitable sites for promotion of the electron exchange. Indeed, the role of edge plane defects of graphene sheets (obtained through anodizing of epitaxial graphene

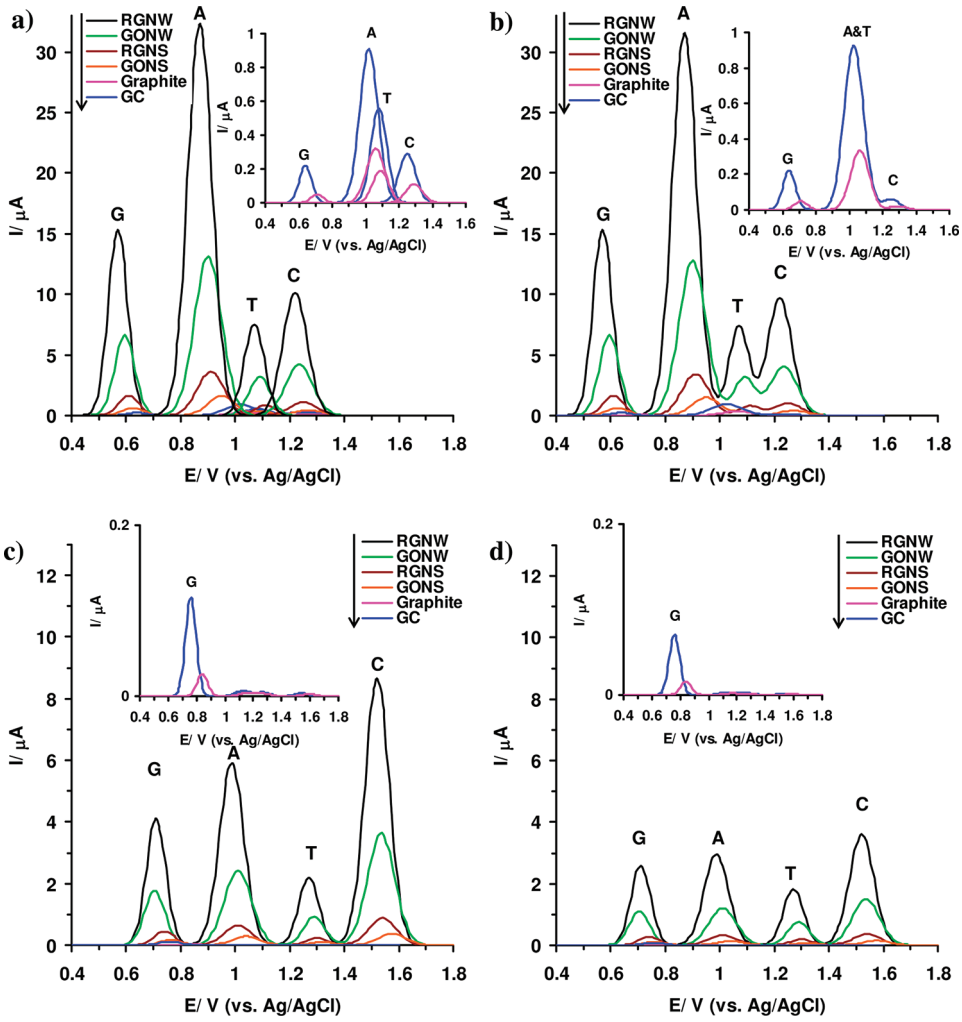

Figure 2. DPV profiles of the RGNW, GONW, RGNS, and GONS electrodes as compared to the graphite and GC electrodes for detection of (a) the four free bases of DNA (G, A, T, and C) separately, (b) an equimolar mixture of G, A, T, and C, (c) ssDNA, and (d) dsDNA, with a concentration of 0.1 μM for all of the species applied in (a)−(d) in 0.1 M PBS as supporting electrolyte at pH 7.0.

sheets) in improvement of the DNA electrochemical sensing was recently studied by Lim *et al.*[57] On the other hand, DNA molecules have a high tendency to get adsorbed on the planar part of the graphene sheets through hydrophobic interactions and $\pi-\pi$ stacking.[61] Therefore, the much better electrochemical performance of the RGNW than the RGNS electrode can be assigned to both the edge plane defects of the vertical nanowalls and their further effective surface area for adsorption of DNA (although the contribution of the planar structure and the edge plane defects of the RGNWs in the electrochemical performance could not be separated).

Figure 2b presents DPV profiles of the graphene-based electrodes as compared to the graphite and GC electrodes for detection of an equimolar mixture of G, A, T, and C with a concentration of 0.1 μM for each one of the species in 0.1 M PBS. The inset of Figure 2b shows that both GC and graphite electrodes cannot be applied for simultaneous detection of all the free DNA bases (see, for example, overlapping of A and T signals). In addition, the C signal located at the higher anodic potentials significantly decreased (as compared to Figure 2a), which can be assigned to fast fouling of the DNA species at the surface of these electrodes at the lower potentials and thus blocking the electrode, as similarly reported by Zhou *et al.*[56] In contrast, the current signals of G, A, T, and C obtained from the graphene-based electrodes were completely separated and distinguishable. Moreover, the signals obtained by the graphene nanowall electrodes (particularly the RGNW electrode) were very strong without any remarkable decrease in the current signals obtained at the higher anodic potentials (as compared to Figure 2a) and overlapping of the signals (as observed for the GC and graphite electrodes). These can be assigned to the high porosity of the graphene nanowalls with an antifouling property and the excellent exchange of electrons at the edge of the nanowalls.

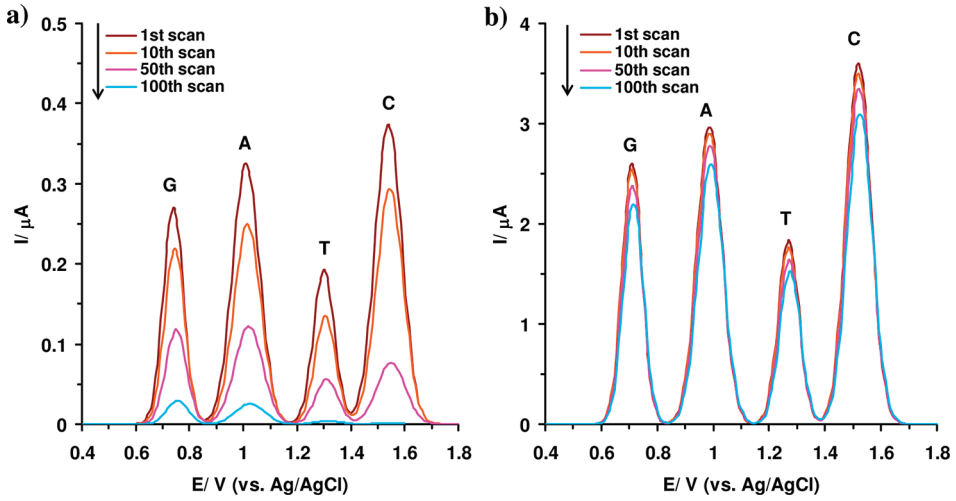

Figure 3. DPV profiles of (a) the RGNS and (b) the RGNW electrodes after increasing the number of scans up to 100 cycles for 0.1 μM dsDNA in 0.1 M PBS as supporting electrolyte at pH 7.0.

Figure 2c and d present DPV profiles of the graphene-based electrodes as compared to the graphite and GC electrodes for detection of ssDNA and dsDNA with a concentration of 0.1 μM in 0.1 M PBS. It is seen that the anodic potentials of the current peaks assigned to oxidation of the DNA bases of the dsDNA are slightly greater than the potential of the ssDNA, and the oxidation potentials of both of them are significantly greater than the potentials observed for the free DNA bases, independent from the kind of applied electrode. This indicates further resistance of the dsDNA and then the ssDNA against oxidation as compared to the free bases. Such resistance resulted in the complete inefficiency of the graphite and GC electrodes, while the graphene-based electrodes (particularly the RGNW electrode) could still show efficient and simultaneous detection of the four bases of the dsDNA. It should be noted that the electrochemical activities of the RGNS, graphite, and GC electrodes in this work were well consistent with the results reported by Zhou *et al.*[56] for chemically reduced graphene oxide modified glassy carbon, graphite/GC, and GC electrodes. This means that we could successfully reproduce the basic results of DNA electrochemical analysis when graphene nanosheet electrodes were used.

The stability of the RGNS and RGNW electrodes during the electrooxidation of the dsDNA was examined by increasing the number of scans up to 100 cycles, as presented in Figure 3. It is seen that the intensity of the current peaks of the RGNS electrode significantly decreased by increasing the number of scan so that after 100 cycles no efficient signals relating to T and C peaks were detected (see Figure 3a). In contrast, the RGNW electrode exhibited a stable behavior with a slight decrease (~15%) in the intensity of the current peaks even after 100 scans. Therefore, the RGNW electrode can provide a facile, reliable, and efficient electrochemical biosensing of DNA.

So far, it was shown that all of the prepared graphene-based electrodes could efficiently work for simultaneous detection of the four bases of dsDNA with a concentration of 0.1 μM, while among them the RGNW electrode exhibited the best performance and efficiency even at a lower concentration of 0.1 nM. Hence, here, we investigated the sensitivity range of the RGNW electrode as compared to the sensitivity of the RGNS electrode to the four DNA bases of the dsDNA at various concentrations, as shown in Figure 4. For the RGNS electrode, it was found that by increasing the concentration of the dsDNA to 10 mM, the T signal disappeared and the C signal significantly diminished (see Figure 4a), which can be assigned to considerable fouling of the DNA species at the surface of the RGNS electrode and blocking the electrode at such a high concentration. On the other hand, the RGNS electrode did not show any considerable sensitivity to the dsDNA with concentrations lower than 2.0 pM. These results indicated that the RGNS electrode cannot act as an efficient DNA biosensor at low (<2.0 pM) and high (≥10 mM) concentrations of dsDNA. However, Figure 4b shows that the RGNW electrode not only can work at the high concentration of 10 mM (without any reduction in the intensity of the current peaks, especially at the higher anodic potentials) but also can detect dsDNA at a very low concentration of 0.1 fM. The excellent performance of the RGNW electrode at such high and low concentrations can be assigned to its high surface porosity and the edge plane defects, which inhibited blocking the electrode due to fouling and accelerated the electron exchange through the extremely sharp edges of the reduced nanoflakes, respectively.

Figure 5 presents current response (defined as ratio of the current peak (obtained after subtraction of the

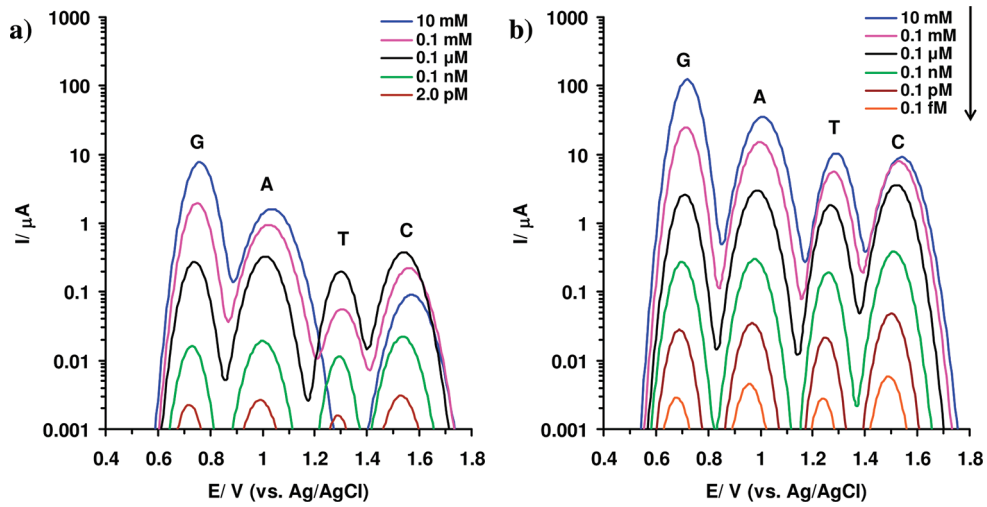

Figure 4. Logarithmic presentation of DPV profiles of (a) the RGNS and (b) RGNW electrodes for detection of various concentrations of dsDNA in 10 M PBS as supporting electrolyte at pH 7.0.

background current in DPV) to the typical current resolution (here, ~1 nA)) of the RGNW and RGNS electrodes to the four bases of dsDNA at various concentrations. The technical and statistical deviations of the experimental data for the current response were around 15% so that the corresponding error bars are not observable in the logarithmic scale. Figure 5 shows that the RGNS electrode could efficiently detect the four bases of the dsDNA in a linear trend only in a limited concentration of dsDNA ranging from 2.0 pM to 0.1 μM. No detectable current signals were observed for concentrations lower than 2.0 pM, and simultaneous detection of the four bases of the dsDNA was impossible for concentrations higher than 10 mM. However, the RGNW electrode exhibited an excellent linear behavior for the current response in a wider and more sensitive range of 0.1 fM to 0.1 μM with small deviations from the linear trend for C, T, and then A bases at the higher concentrations ranging from 0.1 μM to 10 mM. Such small deviations can be assigned to slight fouling of the dsDNA among the pores of the nanoflakes at the lower anodic potentials. Nevertheless, the simultaneous detection of the four bases of the dsDNA at such high concentrations was still possible by the RGNW electrode. These results indicated for the first time that the RGNW electrode can extend the lower limit and upper limit of the dsDNA detection of the graphene-based electrodes to 0.1 fM (4 orders of magnitude more sensitive than the sensitivity of the RGNS) and <10 mM, respectively. Moreover, by linear fitting the experimental data, we obtained the following equations:

$$\log(\Delta I/i_0) = (0.316 \pm 0.006)\log C_{DNA}(\mathrm{M}) + (5.637 \pm 0.112) \text{ in } 0.1 \text{ fM} \leq C_{DNA} \leq 0.1\ \mu\mathrm{M}$$

and

$$\log(\Delta I/i_0) = (0.433 \pm 0.008)\log C_{DNA}(\mathrm{M}) + (5.475 \pm 0.109) \text{ in } 2.0 \text{ pM} \leq C_{DNA} \leq 0.1\ \mu\mathrm{M}$$

for the average of current response (average on ΔI of the G, A, T, and C) as a function of the dsDNA concentration for the RGNW and RGNS electrodes, respectively. The estimated lower limit of the dsDNA detection (defined as the concentration that gave a current signal equal to 3 times the standard deviation of the blank signal (~0.2 nA)) of the RGNW and RGNS electrodes was obtained ~9.4 ± 5.4 zM (1 zepto = 10^{-21}) and 5.4 ± 3.5 fM, respectively. This means that the sensitivity of the RGNW electrode to the dsDNA is theoretically so much better (~6 orders of magnitude) than the sensitivity of the RGNS electrode. The estimated sensitivity for the RGNW electrode also corresponds to the capability of detection of only ~5 DNA molecules in each mL of solution.

The influence of the potential scan rate (ν) on the current−potential characteristics of the oxidation was studied to evaluate whether the processes at the surface of the RGNW electrode were under diffusion or adsorption control. By increasing the scan rate from 5 to 150 mV/s, a slight positive shift in the potential of the peaks (~0.1 V) was observed, which confirmed the irreversibility of the oxidation reactions of the four DNA bases. In addition, a linear dependence of the anodic peak current (I_{pa}) on the scan rate was found for the four DNA bases, indicating an adsorption control process. The net I_{pa}, as the adsorption oxidation current at the electrode, can be described by the following equation:[62]

$$I_{pa} = (nFQ\nu)/4RT$$

where n, F,Q, R, and T are the number of electrons involved in the oxidation reaction, the Faraday constant, the charge involved in the reaction, the gas constant, and the temperature, respectively. The values of n for oxidation of G, A, T, and C were estimated as 1.96, 1.55, 1.12, and 0.92, respectively. These results

suggested that in the oxidation reactions of G and A two electrons could effectively be involved, while in the oxidation reactions of T and C one electron was involved. The complex mechanism describing the electrochemical oxidation of free guanine base, through loss of four total electrons and protons, is schematically exhibited in Figure 6a.[63,64] On the basis of this mechanism, at first, the G molecule loses two electrons and protons followed by a chemical step to form 8-oxoguanine. Then, the produced 8-oxoguanine can undergo a further reversible oxidation through loss of two other electrons and protons. Since the oxidation potential of 8-oxoguanine is substantially lower than that of guanine, the electrochemical oxidation of 8-oxoguanine is highly driven after its formation.[65] The electrochemical oxidation mechanism of free adenine can be described through loss of six total electrons and protons, as schematically presented in Figure 6b.[66] Similar to the oxidation of G, the potentials required for oxidation of the products of the first two oxidations of adenine are substantially lower than the potential needed for oxidation of adenine molecule in the first step.[67] The oxidation reactions of free thymine[68,69] and cytosine[70] bases are also schematically shown in Figure 6c and d, based on the involvement of one electron in the electrochemical oxidation of T and C, respectively.

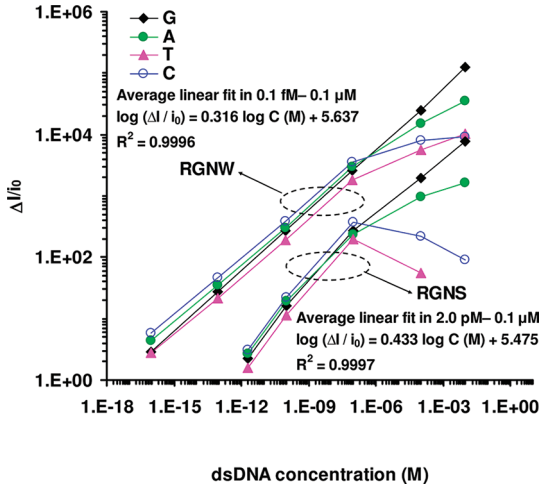

Figure 5. Log–log plot of the current response of the RGNW and RGNS electrodes to the four bases (G, A, T, and C) of the dsDNA at various concentrations. The average linear equations and R^2 are also shown in the inset.

A DNA biosensor should also provide rapid and sensitive detection of SNPs. In fact, SNP is a change in DNA sequence by variation of a single nucleotide in the genome. In addition, based on the results obtained through extrapolation of the experimental data in Figure 5, the sensitivity performance of the RGNW electrodes at single-DNA levels had to be checked. Concerning this, Figure 7 shows DPV profiles of the RGNW electrode for detection of a base oligonucleotide (O#1) with the sequence 5′-CAT-GAA-CCG-3′ and its single-base mismatched oligonucleotides O#2 and O#3 with sequences of 5′-CAT-GAA-CCA-3′ (G → A mutation relative to O#1) and 5′-CAT-GAA-CTG-3′ (C → T mutation relative to O#1), respectively. The DPV profiles were obtained through averaging on data points of 20 sequent DPVs for detection of SNPs of oligonucleotides with a concentration of 20 zM (corresponding to detection of ~10 oligonucleotides/mL). The total time required for completion of the 20 sequent DPVs was about 50 min. The G → A and C → T mutations are distinguishable through comparison of the DPVs of O#2 and O#3 with the DPVs of O#1. Therefore, the prepared RGNW electrode was also efficient in detection of SNPs of short oligomers having a specific sequence, without use of any hybridization and/or labeling processes at an ultra-low concentration of 20 zM. It should be noted that, although

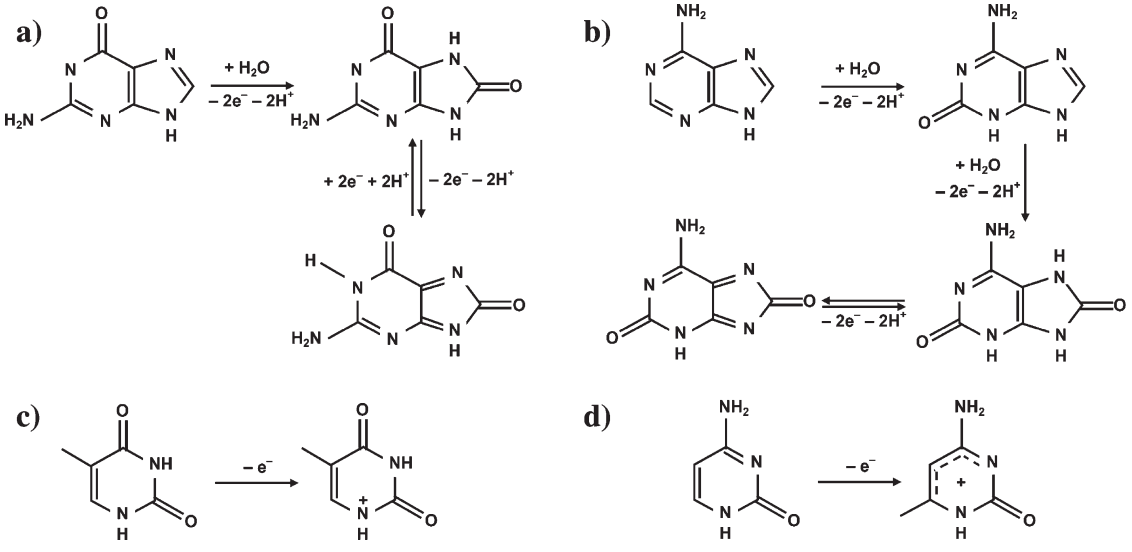

Figure 6. Reaction mechanisms for electrochemical oxidation of (a) G, (b) A, (c) T, and (d) C.

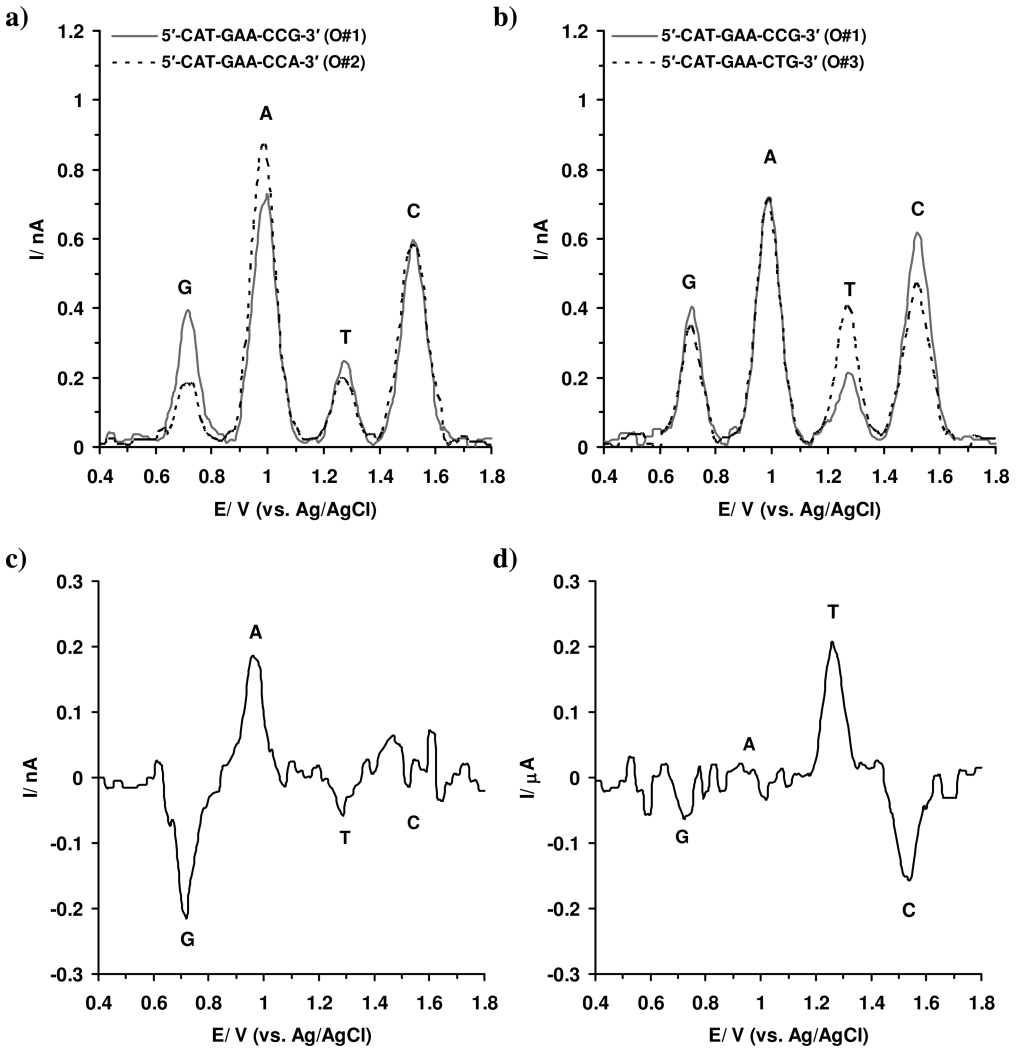

Figure 7. Detection of SNPs of oligonucleotides by using DPVs of the single-base mismatched oligonucleotides obtained through (a) G → A mutation (O#2) and (b) C → T mutation (O#3), as compared to the base oligonucleotide (O#1) at the surface of the RGNW electrode. (c) and (d) present subtraction of the DPVs shown in (a) and (b), respectively. Concentration of the different oligonucleotides was 20 zM in 0.1 mM PBS at pH 7.0.

concentrations of the applied oligonucleotides were identical, for more precision, the peak currents of the DPV profiles were normalized by using the nonmutational bases C and A of O#1 in the DPVs of O#2 and O#3, respectively. This means that the SNPs are detectable by subtraction of DPVs even if the concentrations of the base oligonucleotide and its mismatched type are different, as previously reported by Zhou *et al.*,[56] but for a much higher concentration of the oligonucleotides (~1 μM) using a RGNS-like electrode. The C and A peaks in Figure 7a and b show a nearly perfect overlapping, because they are normalized peaks, respectively. However, the T and G peaks were not exactly overlapped in all runs. Therefore, in Figure 7 we present averaged peaks that were obtained by averaging on all the data points acquired through ~20 similar separate runs. It was also found that the relative standard deviation of the averaged T and G peaks of Figure 7a and b was about 15%. This deviation confirms reliability the detection of the SNPs of the oligonucleotides by using the RGNW electrode at single-DNA levels. By using the same procedure, the capability of the RGNW electrode for detection of the dsDNA molecules in a solution with a concentration of 20 zM was also tested.

Figure 8 shows that by decreasing the concentration of the oligonucleotides to 5 zM, no suitable current signals could be observed for the G and T peaks. This means that no meaningful SNP analysis is possible at such a low concentration. In addition, these results are consistent with the lower limit of detection calculated from the data given in Figure 6. The stability in performance of each RGNW electrode for detection of the oligonucleotides with a concentration of 20 zM was also examined. It was found that after 10 separate runs (*i.e.*, 200 DPVs) the current peaks reduced ~35%. In addition, the standard deviation of the current peaks

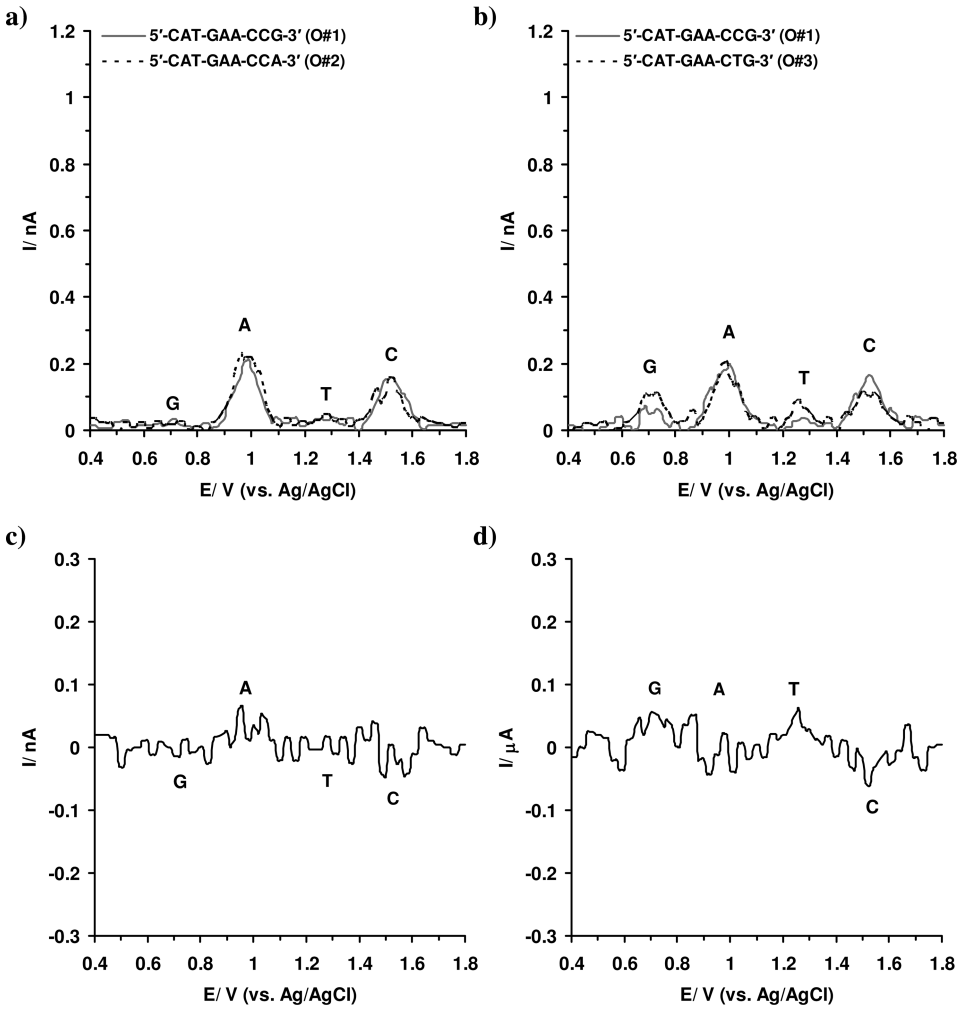

Figure 8. Detection of SNPs of oligonucleotides by using DPVs of the single-base mismatched oligonucleotides obtained through (a) G → A mutation (O#2) and (b) C → T mutation (O#3), as compared to the base oligonucleotide (O#1) at the surface of the RGNW electrode. (c) and (d) present subtraction of the DPVs shown in (a) and (b), respectively. Concentration of the different oligonucleotides was 5.0 zM in 0.1 mM PBS at pH 7.0.

from batch to batch of the RGNW electrodes was obtained as ~25% for $n = 6$.

One can also check that the experimentally obtained lower detection limit of ~10 oligonucleotides/mL is principally consistent with the current theoretical estimations. For example, it is known that due to the presence of cations (as counterions) in a DNA solution, the electrostatic potential of each DNA molecule (with a negative charge) exponentially drops to zero as its distance increases from the surface of the electrode. This screening effect can be quantified by the Debye length (λ_D) as follows:[71]

$$\lambda_D = (\varepsilon kT/1000N_A e^2 \sum_i C_i z_i^2)^{1/2}$$

in which λ_D is defined as the distance at which the electrostatic potential drops to $1/e$ of the potential of the DNA, ε is electrical permittivity of the solution, k is the Boltzmann constant, T is the temperature of the solution in Kelvin, N_A is Avogadro's number, e is the elementary charge, C_i (in molar) is the concentration, and z_i is the valence of the ith ion species. The DNA molecules located far from the Debye length cannot be detected by the electrodes, because of the screening effect caused by counterions.[72] As an estimation, for a solution containing only NaCl with a concentration of 0.1 mM (corresponding to this work), the Debye length is ~100 nm. For the nest-like porous structure of the graphene nanowalls (Figure 1c), this Debye length can be assigned to an effective volume of ~100 nm^3 in which detection of oligonucleotides is theoretically possible. On the other hand, based on Figure 1c, the average pore volume that can be assigned to each nanowall is ~300 nm^3. Thus the probability of detection of each oligonucleotide trapped within one of the pores is ~1/3. Furthermore, the total pore volume of the nanowall electrode was estimated to be ~1.4 × 10^{-2} cm^3. Hence, the probability of detection of one oligonucleotide by the nanowall electrode in one milliliter of the DNA solution after averaging on data acquired through 20 DPVs is ~9 × 10^{-2}. This corresponds to a

TABLE 1. Peak Area (*A*) Ratios of the Oxygen-Containing Bonds to the CC Bonds (by XPS), Peak Intensity Ratios of I_D/I_G (by Raman), and dsDNA Sensitivity (by DPV) of the Graphene-Based Electrodes As Compared to Those of the Graphite Electrode As a Benchmark

	XPS				Raman	DPV	
						dsDNA lower detection limit	
sample	A_{CN}/A_{CC}	A_{COH}/A_{CC}	A_{CO}/A_{CC}	A_{OCOH}/A_{CC}	I_D/I_G	measured	estimated
graphite		0.08 ± 0.04	0.05 ± 0.04		0.09 ± 0.04	~1.0 μM	
GONSs		0.36 ± 0.05	0.74 ± 0.07	0.08 ± 0.04	0.17 ± 0.04	much better than graphite	
RGNSs	0.11 ± 0.04	0.10 ± 0.04	0.11 ± 0.04		0.29 ± 0.05	~2.0 pM	~5.4 ± 3.5 fM
GONWs		0.20 ± 0.05	0.49 ± 0.06	0.09 ± 0.04	0.77 ± 0.07	not better than RGNWs	
RGNWs	0.14 ± 0.04	0.13 ± 0.04	0.19 ± 0.04	0.07 ± 0.04	0.91 ± 0.08	~20 zM	~9.4 ± 5.4 zM

theoretical lower detection limit of ~10 oligonucleotides/mL for definitely detecting one of the oligonucleotides by the graphene nanowall electrode.

It should be noted that the method presented in this work includes some disadvantages, similar to all DNA electrochemical analysis methods. For example, it cannot provide any information on the base sequences of DNA targets and suffers from interferences from any coexistent DNA. Furthermore, it cannot give reliable SNP analyses for long DNA strands, because changes of a couple of bases do not cause a significant signal difference when a DNA strand gets longer. Therefore, the main advantage of this work concentrates on dramatically improvomg the sensitivity of the DNA electrochemical analysis for detection and the SNP analysis of oligonucleotides at single-DNA levels. This means that although the SNP analysis of long DNA strands is very difficult using this method, detection of the long strands is still possible at single levels, based on acquisition of the current signals of its four DNA bases.

CONCLUSIONS

The fabricated GONW electrode (with a very large surface area and edge-plane defects) exhibited much superior electrochemical performances (with sub-fM resolution and high stability even after 100 DPV scans) in label-free detection of the four bases of dsDNA and SNPs of oligonucleotides than the RGNS electrode, which typically showed an electrochemical sensitivity similar to the few graphene-based electrodes studied so far. In fact, the linear dynamic detection range of the RGNW electrode for dsDNA detection was studied in the wide and highly sensitive range of 0.1 fM to 10 mM, while the RGNS electrode showed a narrower linear detection range from 2.0 pM to <10 mM. Using extrapolation of the linear detection range of the electrodes, the lower limit of detection of the RGNW electrode was evaluated as 9.4 zM, while for the RGNS electrode it was found to be 5.4 fM. To check this ultrahigh sensitivity in practice, the RGNWs were successfully used for label-free detection of SNPs of oligonucleotides with a specific sequence at a concentration of 20 zM (equivalent to ~10 DNA/mL). Therefore, the RGNW electrode can realize the first applications of electrochemical sensing and analysis of nucleic acids at single-DNA levels.

EXPERIMENTAL SECTION

Reagents. Natural graphite powder (45 μm, Sigma-Aldrich) was used for synthesis of GO. All of the other chemicals were of analytical reagent grade and were used as received. Distilled water was also used throughout the experiment. The four free bases of DNA, that is, guanine (G), adenine (A), thymine (T), and cytosine (C), and double-stranded DNA from salmon testes were purchased from Sigma Aldrich. Single-stranded DNA was obtained by a prehydrolysis step, which included heating the native ds-DNA solution in a water bath at 100 °C for 5 min followed by rapidly cooling in an ice bath. Oligonucleotides with specific sequences (the sequence from codon 248 of the p53 gene) 5′-CAT-GAA-CCG-3′ (O#1), 5′-CAT-GAA-CCA-3′ (O#2: G → A mutation relative to O#1), and 5′-CAT-GAA-CTG-3′ (O#3: C → T mutation relative to O#1) were obtained through Shanghai Biotechnology Co. Ltd.

Fabrication of RGNW (reduced graphene nanoflakes) Electrodes. At first, GO powder was synthesized by using a modified Hummers method. More details on the synthesis of GO powder by this method were previously reported elsewhere.[33] A GO suspension was prepared by dispersing the prepared GO powder in distilled water (0.1 mg/mL). Then, $Mg(NO_3)_2 + 6H_2O$ as charger was added to the suspension in order to achieve positively charged graphene sheets. The weight ratio of the graphene oxide to the magnesium nitrate was identical. By using this method, a suitable Mg^{2+}-GO electrolyte was obtained for the EPD of the GO nanosheets. A polished stainless steel rod and a graphite rod with a diameter of about 1 mm were used as the electrodes of the EPD. The distance between the two electrodes, the applied voltage, and the deposition time were selected as 5 mm, 30 V, and 10 min, respectively. By applying the negative voltage to the graphite electrode, the positively charged Mg^{2+}-GO sheets were moved toward it for deposition of the GO sheets onto the surface of the electrode in a vertical alignment. The prepared nanoflakes were very fragile, with weak adhesion onto the surface of the electrode, which were their main disadvantages. Some of the prepared GONWs were also reduced by hydrazine to obtain RGNW electrodes.

To have some comparisons, graphene oxide nanosheet (GONS) and reduced graphene nanosheet (RGNS) electrodes

were also prepared. The GONS electrode was prepared by dipping the graphite electrode into a GO suspension (with a concentration of 5 mg/mL) followed by heating at 100 °C in air for 10 min. This deposition process was repeated five times. Some of the prepared GONS electrodes were reduced by hydrazine vapor in a flask for 1 h to obtain RGNS electrodes. The reduction by hydrazine was done after each heat treatment.

Apparatus and Measurements. Surface topography and height profile of the GONSs were studied by AFM (Digital Instruments NanoScope V) in tapping mode. Surface morphology of the graphene-based samples was studied by using a field-emission SEM (Hitachi Co.) operating at 15 kV. XPS was applied to investigate the changes occurring in chemical states of the graphene-based samples. The data were acquired by using a hemispherical analyzer equipped with a monochromatic Al Kα X-ray source ($h\nu = 1486.6$ eV) operating at a vacuum better than 10^{-7} Pa. The XPS peaks were deconvoluted by using Gaussian components after a Shirley background subtraction. Raman spectroscopy was performed at room temperature using a HR-800 Jobin-Yvon with a 532 nm Nd:YAG excitation source to investigate the carbon structure of the graphene-based samples.

DPV was carried out using an Autolab PGSTAT100 potentiostat/galvanostat equipped with a conventional three-electrode electrochemical cell containing a graphene-based electrode, a Pt wire, and an Ag/AgCl electrode with saturated KCl solution as working, counter, and reference electrodes, respectively. The scan rate was adjusted to 10 mV/s. The raw data acquired from the DPV were smoothed at first, and then their baselines were corrected. For detection of single DNA molecules by using the RGNW electrode, in order to obtain the DPV curves with a better signal-to-noise ratio and lower statistical and technical deviations, before smoothing and background subtraction of each curve, we took an average of the data points of 20 separate scans, yielding nearly the same curves through out the same experimental conditions (including the same electrode). In addition to the graphene-based electrode, glassy carbon and graphite electrodes were also used as benchmarks. The GC and graphite electrodes were cleaned by water and ethanol. Then, they were dried in an N_2 environment at 100 °C for 10 min. The supporting electrolyte of the DPV was PBS solution at pH 7.0.

Conflict of Interest: The authors declare no competing financial interest.

Acknowledgment. O.A. would like to thank the Research Council of Sharif University of Technology and also Iran Nanotechnology Initiative Council for financial support of the work.

Supporting Information Available: This information is available free of charge *via* the Internet at http://pubs.acs.org.

REFERENCES AND NOTES

1. McKnight, T. E.; Melechko, A. V.; Guillorn, M. A.; Merkulov, V. I.; Doktycz, M. J.; Culbertson, C. T.; Jacobson, S. C.; Lowndes, D. H.; Simpson, M. L. Effects of Microfabrication Processing on the Electrochemistry of Carbon Nanofiber Electrodes. *J. Phys. Chem. B* **2003**, *107*, 10722–10728.
2. Ding, Y.; Wang, Y.; Lei, Y. Direct Electrochemistry and Electrocatalysis of Novel Single-Walled Carbon Nanotubes-Hemoglobin Composite Microbelts—Towards the Development of Sensitive and Mediator-Free Biosensor. *Biosens. Bioelectron.* **2010**, *26*, 390–397.
3. You, C.; Xu, X.; Tian, B.; Kong, J.; Zhao, D.; Liu, B. Electrochemistry and Biosensing of Glucose Oxidase Based on Mesoporous Carbons with Different Spatially Ordered Dimensions. *Talanta* **2009**, *78*, 705–710.
4. McCreery, R. L. In *Electroanalytical Chemistry*; Bard, A. J., Ed.; Dekker: New York, 1991; Vol. 17, pp 221—374.
5. Bard, A. J.; Faulkner, L. R. *Electrochemical Methods, Fundamentals and Applications*, 2nd ed.; John Wiley and Sons: New York, 2001.
6. Zhang, Y. B.; Tan, Y.; Stormer, H. L.; Kim, P. Experimental Observation of Quantum Hall Effect and Berry's Phase in Graphene. *Nature* **2005**, *438*, 201–204.
7. Novoselov, K. S.; Geim, A. K.; Morozov, S. V.; Jiang, D.; Katsnelson, M. I.; Grigorieva, I. V.; Dubonos, S. V.; Firsov, A. A. Two-Dimensional Gas of Massless Dirac Fermions in Graphene. *Nature* **2005**, *438*, 197–200.
8. Katsnelson, M. I.; Novoselov, K. S. Graphene: New Bridge between Condensed Matter Physics and Quantum Electrodynamics. *Solid State Commun.* **2007**, *143*, 3–13.
9. Gomez-Navarro, C.; Weitz, R. T.; Bittner, A. M.; Scolari, M.; Mews, A.; Burghard, M.; Kern, K. Electronic Transport Properties of Individual Chemically Reduced Graphene Oxide Sheets. *Nano Lett.* **2007**, *7*, 3499–3503.
10. Bai, J.; Zhong, X.; Jiang, S.; Huang, Y.; Duan, X. Graphene Nanomesh. *Nat. Nanotechnol.* **2010**, *5*, 190–194.
11. Akhavan, O. Graphene Nanomesh by ZnO Nanorod Photocatalysts. *ACS Nano* **2010**, *4*, 4174–4180.
12. Wu, Z.-S.; Pei, S.; Ren, W.; Tang, D.; Gao, L.; Liu, B.; Li, F.; Liu, C.; Cheng, H.-M. Field Emission of Single-Layer Graphene Films Prepared by Electrophoretic Deposition. *Adv. Mater.* **2009**, *21*, 1756–1760.
13. Schedin, F.; Geim, A. K.; Morozov, S. V.; Hill, E. W.; Blake, P.; Katsnelson, M. I.; Novoselov, K. S. Detection of Individual Gas Molecules Adsorbed on Graphene. *Nat. Mater.* **2007**, *6*, 652–655.
14. Robinson, J. T.; Perkins, F. K.; Snow, E. S.; Wei, Z. Q.; Sheehan, P. E. Reduced Graphene Oxide Molecular Sensors. *Nano Lett.* **2008**, *8*, 3137–3140.
15. Wang, X.; Zhi, L. J.; Tsao, N.; Tomovic, Z.; Li, J. L.; Mullen, K. Transparent Carbon Films as Electrodes in Organic Solar Cells. *Angew Chem., Int. Ed.* **2008**, *47*, 2990–2992.
16. Gilje, S.; Han, S.; Wang, M.; Wang, K. L.; Kaner, R. B. A Chemical Route to Graphene for Device Applications. *Nano Lett.* **2007**, *7*, 3394–3398.
17. Liang, X.; Fu, Z.; Chou, S. Y. Graphene Transistors Fabricated via Transfer-Printing in Device Active-Areas on Large Wafer. *Nano Lett.* **2007**, *7*, 3840–3844.
18. Stampfer, C.; Schurtenberger, E.; Molitor, F.; Güttinger, J.; Ihn, T.; Ensslin, K. Tunable Graphene Single Electron Transistor. *Nano Lett.* **2008**, *8*, 2378–2383.
19. Bao, W.; Zhang, H.; Bruck, J.; Lau, C. N.; Bockrath, M.; Standley, B. Graphene-Based Atomic-Scale Switches. *Nano Lett.* **2008**, *8*, 3345–3349.
20. Novoselov, K. S.; Geim, A. K.; Morozov, S. V.; Jiang, D.; Zhang, Y.; Dubonos, S. V.; Grigorieva, I. V.; Firsov, A. A. Electric Field Effect in Atomically Thin Carbon Films. *Science* **2004**, *306*, 666–669.
21. Wang, Y.; Lu, J.; Tang, L. H.; Chang, H. X.; Li, J. H. Graphene Oxide Amplified Electrogenerated Chemiluminescence of Quantum Dots and Its Selective Sensing for Glutathione from Thiol-Containing Compounds. *Anal. Chem.* **2009**, *81*, 9710–9715.
22. Hong, W.; Bai, H.; Xu, Y.; Yao, Z.; Gu, Z.; Shi, G. Preparation of Gold Nanoparticle/Graphene Composites with Controlled Weight Contents and Their Application in Biosensors. *J. Phys. Chem. C* **2010**, *114*, 1822–1826.
23. Choi, B. G.; Park, H. S.; Park, T. J.; Yang, M. H.; Kim, J. S.; Jang, S.-Y.; Heo, N. S.; Lee, S. Y.; Kong, J.; Hong, W. H. Solution Chemistry of Self-Assembled Graphene Nanohybrids for High-Performance Flexible Biosensors. *ACS Nano* **2010**, *4*, 2910–2918.
24. Shang, N. G.; Papakonstantinou, P.; McMullan, M.; Chu, M.; Stamboulis, A.; Potenza, A.; Dhesi, S. S.; Marchetto, H. Catalyst-Free Efficient Growth, Orientation and Biosensing Properties of Multilayer Graphene Nanoflake Films with Sharp Edge Planes. *Adv. Funct. Mater.* **2008**, *18*, 3506–3514.
25. Wang, Y.; Shao, Y.; Matson, D. W.; Li, J.; Lin, Y. Nitrogen-Doped Graphene and Its Application in Electrochemical Biosensing. *ACS Nano* **2010**, *4*, 1790–1798.
26. Shan, C. S.; Yang, H. F.; Song, J. F.; Han, D. X.; Ivaska, A.; Niu, L. Direct Electrochemistry of Glucose Oxidase and Biosensing for Glucose Based on Graphene. *Anal. Chem.* **2009**, *81*, 2378–2382.

27. Alwarappan, S.; Liu, C.; Kumar, A.; Li, C.-Z. Enzyme-Doped Graphene Nanosheets for Enhanced Glucose Biosensing. *J. Phys. Chem. C* **2010**, *114*, 12920–12924.
28. Liu, Y.; Yu, D.; Zeng, C.; Miao, Z.; Dai, L. Biocompatible Graphene Oxide-Based Glucose Biosensors. *Langmuir* **2010**, *26*, 6158–6160.
29. Wu, H.; Wang, J.; Kang, X.; Wang, C.; Wang, D.; Liu, J.; Aksay, I. A.; Lin, Y. Glucose Biosensor Based on Immobilization of Glucose Oxidase in Platinum Nanoparticles/Graphene/Chitosan Nanocomposite Film. *Talanta* **2009**, *80*, 403–406.
30. Mohanty, N.; Berry, V. Graphene-Based Single−Bacterium Resolution Biodevice and DNA Transistor: Interfacing Graphene Derivatives with Nanoscale and Microscale Biocomponents. *Nano Lett.* **2008**, *8*, 4469–4476.
31. Du, D.; Zou, Z.; Shin, Y.; Wang, J.; Wu, H.; Engelhard, M. H.; Liu, J.; Aksay, I. A.; Lin, Y. Sensitive Immunosensor for Cancer Biomarker Based on Dual Signal Amplification Strategy of Graphene Sheets and Multienzyme Functionalized Carbon Nanospheres. *Anal. Chem.* **2010**, *82*, 2989–2995.
32. Akhavan, O.; Ghaderi, E. Photocatalytic Reduction of Graphene Oxide Nanosheets on TiO_2 Thin Film for Photoinactivation of Bacteria in Solar Light Irradiation. *J. Phys. Chem. C* **2009**, *113*, 20214–20220.
33. Akhavan, O.; Ghaderi, E. Toxicity of Graphene and Graphene Oxide Nanowalls Against Bacteria. *ACS Nano* **2010**, *4*, 5731–5736.
34. Hu, W.; Peng, C.; Luo, W.; Lv, M.; Li, X.; Li, D.; Huang, Q.; Fan, C. Graphene-Based Antibacterial Paper. *ACS Nano* **2010**, *4*, 4317–4323.
35. Akhavan, O.; Ghaderi, E.; Esfandiar, A. Wrapping Bacteria by Graphene Nanosheets for Isolation from Environment, Reactivation by Sonication and Inactivation by Near-Infrared Irradiation. *J. Phys. Chem. B* **2011**, *115*, 6279–6288.
36. Akhavan, O.; Ghaderi, E. *Escherichia coli* Bacteria Reduce Graphene Oxide to Bactericidal Graphene in a Self-Limiting Manner. *Carbon* **2012**, *50*, 1853–1860.
37. Wilhelm, J.; Pingoud, A. Real-Time Polymerase Chain Reaction. *Chem. Biol. Chem.* **2003**, *4*, 1120–1128.
38. Goodrich, T. T.; Lee, H. J.; Corn, R. M. Enzymatically Amplified Surface Plasmon Resonance Imaging Method Using RNase H and RNA Microarrays for the Ultrasensitive Detection of Nucleic Acids. *Anal. Chem.* **2004**, *76*, 6173–6178.
39. Zhang, K.; Zhang, Y. Lable-Free Electrochemical DNA Sensor Based on Gold Nanoparticles/Poly(neutral red) Modified Electrode. *Electroanalysis* **2010**, *6*, 673–679.
40. Zhang, J.; Song, S.; Zhang, L.; Wang, L.; Wu, H.; Pan, D.; Fan, C. Sequence-Specific Detection of Femtomolar DNA via a Chronocoulometric DNA Sensor (CDS): Effects of Nanoparticle-Mediated Amplification and Nanoscale Control of DNA Assembly at Electrodes. *J. Am. Chem. Soc.* **2006**, *128*, 8575–8580.
41. Ren, R.; Leng, C.; Zhang, S. A Chronocoulometric DNA Sensor Based on Screen-Printed Electrode Doped with Ionic Liquid and Polyaniline Nanotubes. *Biosens. Bioelectron.* **2010**, *25*, 2089–2094.
42. Ferguson, B. S.; Buchsbaum, S. F.; Swensen, J. S.; Hsieh, K.; Lou, X.; Soh, H. T. Integrated Microfluidic Electrochemical DNA Sensor. *Anal. Chem.* **2009**, *81*, 6503–6508.
43. Xiao, Y.; Lubin, A. A.; Baker, B. R.; Plaxco, K. W.; Heeger, A. J. Single-Step Electronic Detection of Femtomolar DNA by Target-Induced Strand Displacement in an Electrode-Bound Duplex. *Proc. Natl. Acad. Sci. U. S. A.* **2006**, *103*, 16677–16680.
44. Hwang, S.; Kim, E.; Kwak, J. Electrochemical Detection of DNA Hybridization Using Biometallization. *Anal. Chem.* **2005**, *77*, 579–584.
45. Bangar, M. A.; Shirale, D. J.; Purohit, H. J.; Chen, W.; Myung, N. V.; Mulchandani, A. Single Conducting Polymer Nanowire Based Sequence-Specific, Base-Pair-Length Dependant Label-Free DNA Sensor. *Electroanalysis* **2011**, *23*, 371–379.
46. Peter, C.; Meusel, M.; Grawe, F.; Katerkamp, A.; Cammann, K.; Brchers, T. Optical DNA-Sensor Chip for Real-Time Detection of Hybridization Events. *Fresenius J. Anal. Chem.* **2001**, *371*, 120–127.
47. Gnanaprakasa, T. J.; Oyarzabal, O. A.; Olsen, E. V.; Pedrosa, V. A.; Simonian, A. L. Tethered DNA Scaffolds on Optical Sensor Platforms for Detection of *hipO* Gene from *Campylobacter jejuni*. *Sens. Actuators B* **2011**, *156*, 304–311.
48. Loaiza, O. A.; Campuzano, S.; Pedrero, M.; Pividori, M. I.; García, P.; Pingarrn, J. M. Disposable Magnetic DNA Sensors for the Determination at the Attomolar Level of a Specific *Enterobacteriaceae* Family Gene. *Anal. Chem.* **2008**, *80*, 8239–8245.
49. Drummond, T. G.; Hill, M. G.; Barton, J. K. Nat. Electrochemical DNA Sensors. *Biotechnology* **2003**, *21*, 1192–1199.
50. Sassolas, A.; Leca-Bouvier, B. D.; Blum, L. J. DNA Biosensors and Microarrays. *Chem. Rev.* **2008**, *108*, 109–139.
51. Wang, J.; Kawde, A. N. Amplified Label-Free Electrical Detection of DNA Hybridization. *Analyst* **2002**, *127*, 383–386.
52. Jelen, F.; Yosypchuk, B.; Kourilová, A.; Novotn, L.; Paleček, E. Label-Free Determination of Picogram Quantities of DNA by Stripping Voltammetry with Solid Copper Amalgam or Mercury Electrodes in the Presence of Copper. *Anal. Chem.* **2002**, *74*, 4788–4793.
53. Niwa, O.; Jia, J.; Sato, Y.; Kato, D.; Kurita, R.; Maruyama, K.; Suzuki, K.; Hirono, S. Electrochemical Performance of Angstrom Level Flat Sputtered Carbon Film Consisting of sp^2 and sp^3 Mixed Bonds. *J. Am. Chem. Soc.* **2006**, *128*, 7144–7145.
54. Kato, D.; Sekioka, N.; Ueda, A.; Kurita, R.; Hirono, S.; Suzuki, K.; Niwa, O. A Nanocarbon Film Electrode As a Platform for Exploring DNA Methylation. *J. Am. Chem. Soc.* **2008**, *130*, 3716–3717.
55. Kato, D.; Sekioka, N.; Ueda, A.; Kurita, R.; Hirono, S.; Suzuki, K.; Niwa, O. Nanohybrid Carbon Film for Electrochemical Detection of SNPs without Hybridization or Labeling. *Angew. Chem., Int. Ed.* **2008**, *47*, 6681–6684.
56. Zhou, M.; Zhai, Y.; Dong, S. Electrochemical Sensing and Biosensing Platform Based on Chemically Reduced Graphene Oxide. *Anal. Chem.* **2009**, *81*, 5603–5613.
57. Lim, C. X.; Hoh, H. Y.; Ang, P. K.; Loh, K. P. Direct Voltammetric Detection of DNA and pH Sensing on Epitaxial Graphene: An Insight into the Role of Oxygenated Defects. *Anal. Chem.* **2010**, *82*, 7387–7393.
58. Dubuisson, E.; Yang, Z.; Loh, K. P. Optimizing Label-Free DNA Electrical Detection on Graphene Platform. *Anal. Chem.* **2011**, *83*, 2452–2460.
59. Akhavan, O.; Ghaderi, E. Copper Oxide Nanoflakes as Highly Sensitive and Fast Response Self-Sterilizing Biosensors. *J. Mater. Chem.* **2011**, *21*, 12935–12940.
60. Soleymani, L.; Fang, Z.; Sun, X.; Yang, H.; Taft, B. J.; Sargent, E. H.; Kelley, S. O. Nanostructuring of Patterned Microelectrodes To Enhance the Sensitivity of Electrochemical Nucleic Acids Detection. *Angew. Chem., Int. Ed.* **2009**, *48*, 8457–8460.
61. Wu, M.; Kempaiah, R.; Huang, P. J. J.; Maheshwari, V.; Liu, J. Adsorption and Desorption of DNA on Graphene Oxide Studied by Fluorescently Labeled Oligonucleotides. *Langmuir* **2011**, *27*, 2731–2738.
62. Wang, J. *Analytical Electrochemistry*, second ed.; Wiley-VCH: New York, 2000.
63. Goyal, R. N.; Dryhurst, G. Redox Chemistry of Guanine and 8-Oxyguanine and a Comparison of the Peroxidase-Catalyzed and Electrochemical Oxidation of 8-Oxyguanine. *J. Electroanal. Chem.* **1982**, *135*, 75–91.
64. Li, Q.; Batchelor-McAuley, C.; Compton, R. G. Electrochemical Oxidation of Guanine: Electrode Reaction Mechanism and Tailoring Carbon Electrode Surfaces To Switch between Adsorptive and Diffusional Responses. *J. Phys. Chem. B* **2010**, *114*, 7423–7428.
65. Oliveira Brett, A. M.; Piedade, J. A. P.; Serrano, S. H. P. Electrochemical Oxidation of 8-Oxoguanine. *Electroanalysis* **2000**, *12*, 969–973.
66. Gonçalves, L. M.; Batchelor-McAuley, C.; Barros, A. A.; Compton, R. G. Electrochemical Oxidation of Adenine: A Mixed Adsorption and Diffusion Response on an Edge-

Plane Pyrolytic Graphite Electrode. *J. Phys. Chem. C* **2010**, *114*, 14213–14219.
67. Oliveira-Brett, A. M.; Diculescu, V.; Piedade, J. A. P. Electrochemical Oxidation Mechanism of Guanine and Adenine Using a Glassy Carbon Microelectrode. *Bioelectrochemistry* **2002**, *55*, 61–62.
68. Wang, Z.; Wang, Y.; Luo, G. The Electrocatalytic Oxidation of Thymine at α-Cyclodextrin Incorporated Carbon Nanotube-Coated Electrode. *Electroanalysis* **2003**, *15*, 1129–1133.
69. Sun, W.; Xi, M.; Zhang, L.; Zhan, T.; Gao, H.; Jiao, K. Electrochemical Behaviors of Thymine on a New Ionic Liquid Modified Carbon Electrode and Its Detection. *Electrochim. Acta* **2010**, *56*, 222–226.
70. Wagner, R.; Cadet, J. Oxidation Reactions of Cytosine DNA Components by Hydroxyl Radical and One-Electron Oxidants in Aerated Aqueous Solutions. *Acc. Chem. Res.* **2010**, *43*, 564–571.
71. Kataoka-Hamai, C.; Miyahara, Y. Label-Free Detection of DNA by Field-Effect Devices. *IEEE Sens. J.* **2011**, *11*, 3153–3160.
72. Stern, E.; Wagner, R.; Sigworth, F. J.; Breaker, R.; Fahmy, T. M.; Reed, M. A. Importance of the Debye Screening Length on Nanowire Field Effect Transistor Sensors. *Nano Lett.* **2007**, *7*, 3405–3409.